Progress In Electromagnetics Research, Vol. 145, 175–183, 2014

Polarization-insensitive Triple-Band Microwave Metamaterial Absorber Based on Rotated Square Rings

Guo-Dong Wang[1], Jun-Feng Chen[1], Xi-Wei Hu[1], Zhao-Quan Chen[2, 3], and Ming-Hai Liu[1, *]

Abstract—An ultra-thin triple-band metamaterial absorber (MA) is proposed in the microwave region, which is composed of a periodic array of three rotated square rings (RSRs) and a continuous metal film separated by only 1 mm dielectric substrate. The fabricated MA exhibits three experimental absorption peaks at 4.88 GHz, 7.88 GHz, and 11.32 GHz with the corresponding absorption rates of 98.8%, 96.5%, and 95.9%, which shows an excellent agreement with the simulated results. The triple-band MA is polarization-insensitive at the normal incidence. Finally, the multi-reflection interference theory is introduced to interpretate the absorption mechanism. The calculated absorption rates of the improved unit cell for the strongly coupled MA coincide well with the simulated results at wide angles of incidence for both transverse electric (TE) and transverse magnetic (TM) waves.

1. INTRODUCTION

Over the past several years, electromagnetic (EM) metamaterials (MMs) with perfect absorption have attracted great interest from scientists in many research fields. The original work of ultra-thin metamaterial absorber (MA) was proposed by Bilotti et al. in the microwave region. That absorber consisted of an array of split ring resonators (SRRs) and a resistive sheet to absorb EM energy of the incident wave at the resonance frequency [1]. In 2008, Landy et al. experimentally demonstrated a perfect MA at 11.5 GHz, which was composed of a sub-wavelength sandwiched structure of electric ring resonators (ERRs), a dielectric substrate, and metal cut wires [2]. However, the high absorption of the MA is generally based on electromagnetic resonances, so its working bandwidth is relatively narrow. Recently, most of efforts are made on MAs to achieve polarization-insensitive absorption [3–5], wide-angle absorption [6–8], multi-band absorption [9–14], and broadband absorption [15–18]. Up to now, the MAs have been demonstrated in every technologically relevant spectral range, from the microwave region [1–5, 9–14, 17, 18], the terahertz region [6, 15, 16], to the infrared region [7, 19], and even to the optical region [8, 20].

The generally accepted idea is that by manipulating the electric and magnetic resonances of the MA independently, it is possible to achieve $\varepsilon = \mu$, matching its impedance to the free space, and attain a large imaginary part in the refraction index n_2 simultaneously. Both the reflection and transmission waves are minimized at the same frequency and hence the absorption is maximized with the incident energy being converted into heat. However, the sandwiched MA can hardly be treated a homogenous material due to its inhomogeneity in the wave propagating direction and is not strictly characterized by the effective medium theory. Additionally, this theory can't study the interactions between the two metallic layers and therefore only qualitatively analyze the absorption mechanism. Recently, the interference theory is proposed to analyze uncoupled MAs where the near-field coupling between the two metallic layers

Received 4 January 2014, Accepted 8 March 2014, Scheduled 18 March 2014

* Corresponding author: Minghai Liu (mhliu@mail.hust.edu.cn).

[1] State Key Laboratory of Advanced Electromagnetic Engineering and Technology, Huazhong University of Science and Technology, Wuhan 430074, China. [2] University ITMO, Kronverkskiy pr. 49, St. Petersburg 197101, Russia. [3] College of Electrical and Information Engineering, Anhui University of Science and Technology, Huainan 232001, China.

is insignificant [9, 21–23]. For strongly coupled MAs, compensated patches are introduced to obtain the parasitic capacitance from the metal film and therefore the near-field coupling gets back [24]. As a result, we adopt the interference theory to analyze the absorption mechanism qualitatively.

In this paper, we investigate the absorption rates of the microwave triple-band MA numerically and experimentally, which consists of a periodic array of three rotated square rings (RSRs) and a continuous metal film separated by a dielectric substrate. Experimental results show that the MA exhibits three absorption peaks at 4.88 GHz, 7.88 GHz, and 11.32 GHz with the corresponding absorption rates of 98.8%, 96.5%, and 95.9%, which are in excellent agreement with the simulated results. This MA could operate well at different angles of incidence for both transverse electric (TE) and transverse magnetic (TM) waves. Finally, the multi-reflection interference theory is used to interpretate the absorption mechanism of the single-band MA. The calculated absorption rates of the improved unit cell agree well with the simulated and experimental results. Moreover, the interference theory is also effective for the strongly coupled MA at wide angles of incidence for both TE and TM waves.

2. DESIGN, SIMULATION, AND EXPERIMENT OF TRIPLE-BAND MA

The schematic diagram and geometric parameters of the triple-band MA unit cell are illustrated in Figure 1(a). The unit cell consists of a sandwiched structure of three metallic RSRs, a dielectric substrate, and a continuous metal film. The top RSR structure is obtained by three closed square rings with a 45-degree rotation, which strongly couples to the incident electric filed and exhibits a pure electric

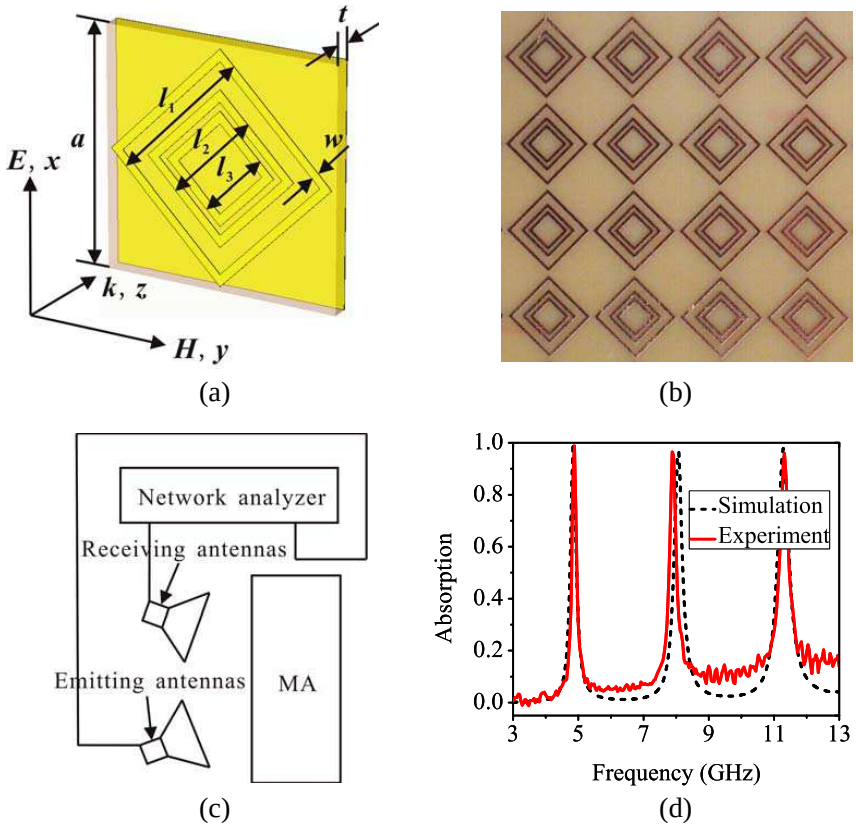

Figure 1. (a) Schematic diagram and geometric parameters of the triple-band MA unit cell with axes indicating the polarization and propagation directions of the incident wave. (b) Photograph of a portion of the fabricated triple-band absorber. (c) Schematic diagram of reflection measurement. The emitting and receiving horn antennas are connected to a network analyzer with low loss flexible cables. (d) Simulated and experimental absorption rates of the triple-band MA.

response as counter-circulating currents in the unit cell eliminate any magnetoelectric response [25]. The incident magnetic field couples to the two metallic layers on both sides of dielectric substrate, which exhibits a magnetic resonance [9, 15]. We can obtain tailored electric and magnetic resonances at the same frequency by tuning geometric parameters of the unit cell and achieve a near-unity absorption. Because the RSR resonator possesses its fourfold rotational symmetry about the propagation axis, the triple-band MA is polarization-insensitive at the normal incidence [3–5].

The proposed MA is designed and optimized by CST Microwave Studio, which is based on the commercial finite difference time domain (FDTD) solver. Periodic boundary condition is set along the lateral directions of the MA and open boundary condition is set along the wave propagating direction. Frequency domain solver and hexahedral mesh are applied in our design. A lossy FR-4 substrate with relative permittivity $\varepsilon_r = 3.5$ and loss tangent $\tan\delta = 0.025$ is used. The metallic material is copper with electric conductivity $\sigma = 5.8 \times 10^7\,\mathrm{S/m}$. The final optimized geometry of the unit cell is given by: $a = 14\,\mathrm{mm}$, $l_1 = 9.5\,\mathrm{mm}$, $l_2 = 6.3\,\mathrm{mm}$, $l_3 = 4.6\,\mathrm{mm}$, $w = 0.5\,\mathrm{mm}$, and $t = 1.0\,\mathrm{mm}$. The transmission is zero in the whole frequency range due to the shielding of the copper film and thus the reflection is the only factor determining the absorption. Therefore, the absorption rate is calculated by $A(w) = 1 - R(w) = 1 - |S_{11}|^2$ [2]. The simulated absorption rate of the triple-band MA is shown in Figure 1(d). It is easily seen that three distinct absorption peaks are obtained at 4.84 GHz, 8.06 GHz, and 11.28 GHz with the absorption rates of 99.9%, 97.9%, and 97.8%, respectively.

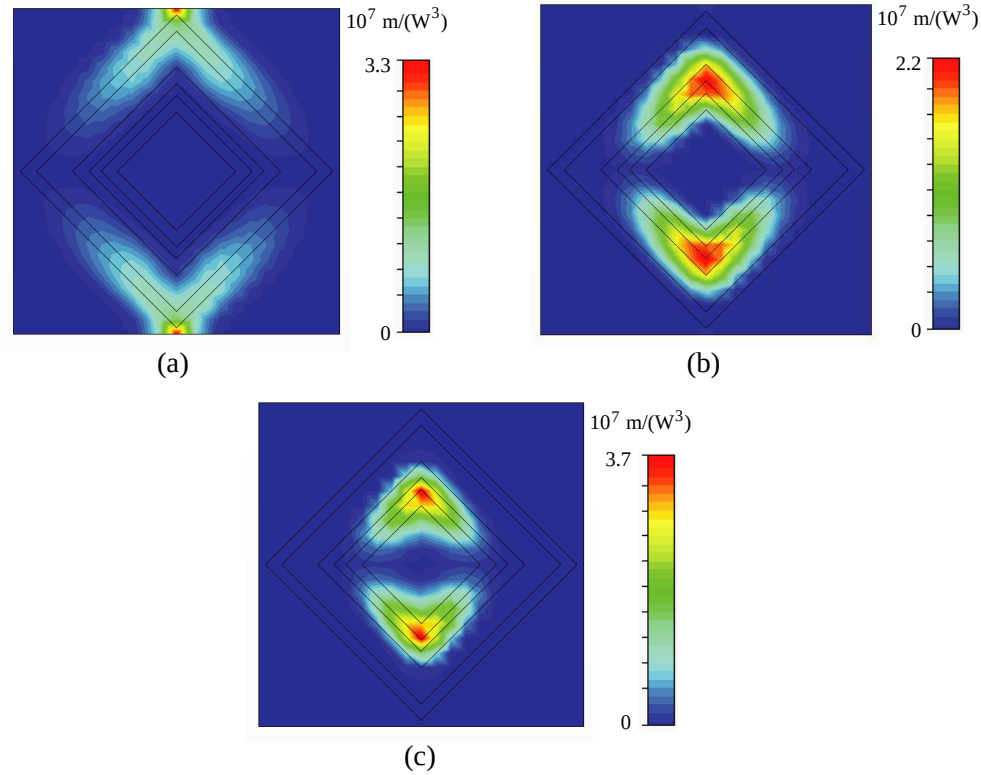

Figure 2. Distributions of the power-loss density in the triple-band MA at the resonance frequencies of (a) 8.84 GHz, (b) 9.8 GHz, and (c) 11.72 GHz.

The MA was fabricated into a 280 mm × 280 mm sample by printed circuit board (PCB) technology as shown in Figure 1(b). The MA sample was characterized through free space reflection measurements in a microwave anechoic chamber. Figure 1(c) depicts the schematic diagram of reflection measurement. An Agilent PNA-X N5244A vector network analyzer and two broadband horn antennas were connected by a coaxial cable. Two antennas were used to emit and receive the electromagnetic wave. Many pyramid absorbing materials were placed around the MA sample to eliminate the electromagnetic interference from the surrounding environment. The distance between the sample and the antennas was set at about

2.5 m to avoid the near-field effect. A bare aluminum board with the same sizes as the sample was used as a calibration. The ratio of the reflection coefficients between the sample and the aluminum board was regarded as the reflection coefficient of the MA. The polarization-insensitive feature is characterized by rotating the antenna polarization angle from 0° to 45°. As shown in Figure 1(d), the fabricated MA exhibits three perfect experimental absorption peaks at 4.88 GHz, 7.88 GHz, and 11.32 GHz with the corresponding absorption rates of 99.9%, 97.9%, and 97.8%, which shows an excellent agreement with our simulated results. Additionally, a 180 MHz frequency redshift in the second resonance occurs, which may be due to fabrication accuracy and measurement errors.

The simulated power-loss density distributions in the triple-band MA are monitored in Figure 2, where Figures 2(a), 2(b), and 2(c) represent the power loss distributions of the incident wave at 4.84 GHz, 8.06 GHz, and 11.28 GHz, respectively. In Figure 2, each distribution of the power-loss density corresponds to a resonance frequency point and a RSR structure. Most of the power loss takes place in the upper and lower parts of the RSR and the dielectric losses occur in between the two metallic layers where the EM field is very large [2, 9]. It is easily observed that the larger-size RSR corresponds to a lower-frequency resonance, while the smaller-size RSR corresponds to a higher-frequency resonance. This resonance characteristics are similar to those of the cut wires and circular patch structures [15, 16]. Therefore, the MA with three RSRs of different geometric parameters can achieve a perfect triple-band absorption.

To better study the polarization-insensitive feature of the proposed MA, we plot the simulated and experimental absorption rates at an polarization angle of 45° under the normal incidence, as given in Figure 3. The absorber shows three experimental absorption peaks at 4.88 GHz, 7.88 GHz, and 11.32 GHz with the corresponding absorption rates of 98.6%, 97.8%, and 95.5%, which agrees well

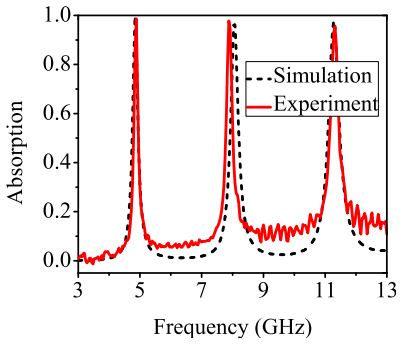

Figure 3. Simulated and experimental absorption rates of the triple-band MA at an polarization angle of 45° under the normal incidence.

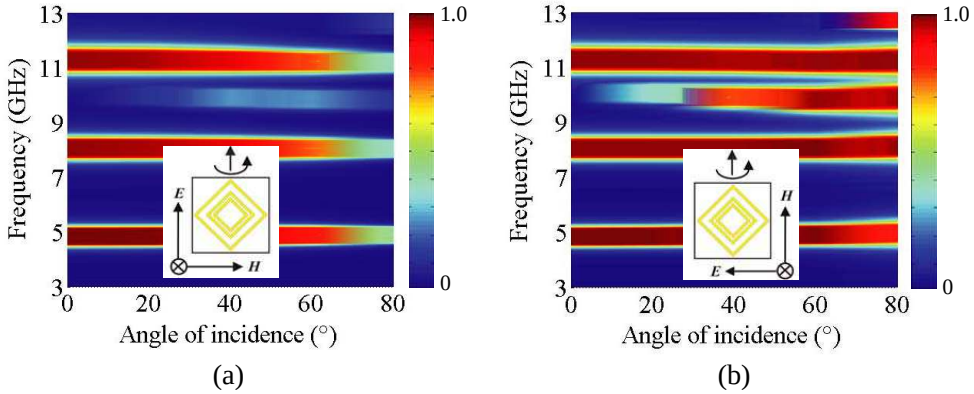

Figure 4. Simulated absorption rates of the triple-band MA at different angles of incidence for (a) TE and (b) TM waves. The insets indicate the polarization and propagation directions of the incident wave.

with the simulated results and those shown in Figure 1(c). These results validate that this absorber is polarization-insensitive at the normal incidence. The absorption rates of the triple-band MA at different angles of incidence for TE and TM waves are depicted in Figure 4. For the case of TE wave shown in Figure 4(a), three perfect peaks at 4.88 GHz, 7.88 GHz, and 11.32 GHz are achieved at the normal incidence. With the increasing angle of incidence, the peaks slightly decrease and have respective absorption rates of 84.2%, 75.7%, and 76.6% at an incidence angle of 60°. When the incident angle further increases, the peaks suddenly decrease, as the y component of the incident magnetic field drops rapidly to zero and can no longer effectively induce a strong magnetic resonance. For the TM case given in Figure 4(b), the absorption rates almost remain the same at the three resonance frequencies. This is because the direction of the incident magnetic field remains unchanged at different angles of incidence and it can efficiently drive a strong magnetic resonance. It should be noted that an additional absorption peak appears at the frequency of about 9.8 GHz at wide incidence angles from 30° to 80° for the TM wave, which is mainly caused by a higher-frequency resonance of the larger-sized RSR structure. These results demonstrate that the triple-band MA could achieve high absorption rates at wide angles of incidence for both TE and TM waves.

3. MULTI-REFLECTION INTERFERENCE THEORY

For simplicity, we only take the lower-frequency resonance for example. In the following, the single-band MA with only the large-size RSRs is proposed. In contrast to the original triple-band MA, the two lower-size RSR structures are removed and the others keep unchanged, as illustrated in Figure 5(a). The MA unit cell consists of the larger-sized RSR and a continuous metal film separated by a dielectric substrate. This absorber was fabricated into a 180 mm × 180 mm sample as presented in Figure 5(b).

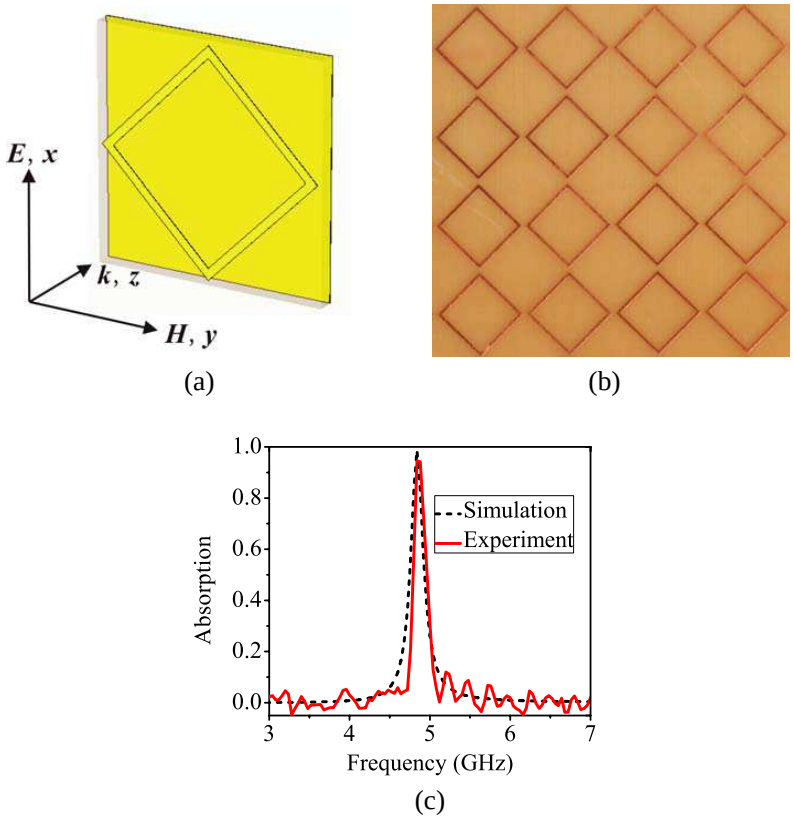

Figure 5. (a) Schematic diagram of the single-band MA unit cell with axes indicating the polarization and propagation directions of the incident wave. (b) Photograph of a portion of the fabricated single-band absorber. (c) Simulated and experimental absorption rates of the single-band MA.

Figure 5(c) gives the simulated and experimental absorption rates of the single-band MA. The fabricated MA has an absorption peak of 94.6% at 4.84 GHz, which agrees well with the simulated results.

For an uncoupled MA, it can be treated as a decoupled system where the near-field coupling between the RSR array and the copper film can be neglected. As depicted in Figure 6, the MA system contains two interfaces: one is the RSR layer and the other is the copper film. The RSR resonator acts as a part of the reflection surface which can reflect/transmit a part of the incident wave. The copper film works as a perfect reflector with a reflection coefficient of -1, i.e., $S_{23} = -1$, and therefore the transmission through the MA is zero. The total reflection is the superposition of the multiple reflections at the RSR interface:

$$\begin{aligned} S_{11\text{total}} &= S_{11} + S_{21}e^{ikd}S_{23}e^{ikd}S_{12} + S_{21}e^{ikd}S_{23}e^{ikd}\left(S_{22}e^{ikd}S_{23}e^{ikd}\right)S_{12} \\ &\quad + S_{21}e^{ikd}S_{23}e^{ikd}\left(S_{22}e^{ikd}S_{23}e^{ikd}\right)^2 S_{12} + \ldots \\ &= S_{11} + S_{12}S_{21}S_{23}e^{i2kd}\sum_{n=0}^{\infty}\left(S_{22}S_{23}e^{i2kd}\right)^n = S_{11} - \frac{S_{12}S_{21}e^{i2kd}}{1 + S_{22}e^{i2kd}} \end{aligned} \tag{1}$$

where S_{11}, S_{22}, S_{12}, and S_{21} are the reflection and transmission coefficients of the RSR interface, k is the corresponding propagation wavenumber, $d = t/\cos(\arcsin(\sin\alpha/\sqrt{\varepsilon}))$ is the propagation distance of the transmitting wave from the RSR layer to the metal film, α is the angle between the incidence wave and the normal of the RSR interface, and ε is the complex permittivity of the dielectric substrate.

To attain a near-unity absorption at the resonance frequency, i.e., the reflection coefficient is almost zero. We simulate the isolated RSR layer by CST Microwave Studio. As illustrated in Figure 7(a), the copper film is removed from the unit cell shown in Figure 5(a) and the thicknesses of air and the FR4 substrate are set to 7.5 mm. In Figure 8, an analytical absorption peak of 98.2% at 5.38 GHz is achieved using the original unit cell. Compared with the simulated and experimental results, the frequency

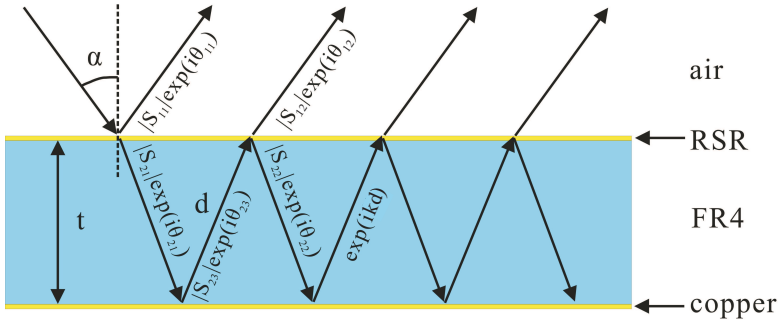

Figure 6. The interference model of the single-band MA and associated geometric parameters.

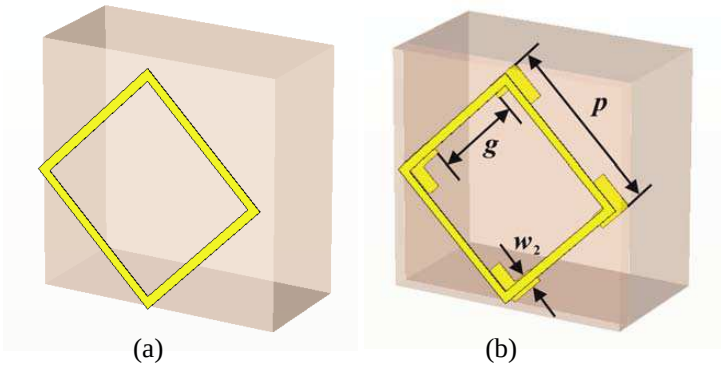

Figure 7. (a) Original and (b) improved unit cells used to simulate S-parameters at the RSR interface.

blueshift of about 0.54 GHz occurs, which is caused by the neglection of the near-field coupling between the two metallic layers. Next, we introduce four copper patches into the unit cell to compensate parasitic capacitance from the copper film and therefore the near-field coupling between two metallic layers gets back. Figure 7(b) plots the improved unit cell, whose additional parameters are given as follows: $p = 9.85$ mm, $g = 5.4$ mm, and $w_2 = 0.85$ mm. In Figure 8, a perfect absorption peak is achieved at the frequency of 4.83 GHz. This calculated absorption rates using the improved unit cell coincide well with the simulated and experimental results given in Figure 5(c). As a result, this method provides a robust and rational physical insight into the absorption mechanism at the normal incidence.

The simulated absorption rates of the single-band MA at different angles of incidence for both TE and TM waves are plotted in Figures 9(a) and 9(b). For the TM wave in Figure 9(b), a similar

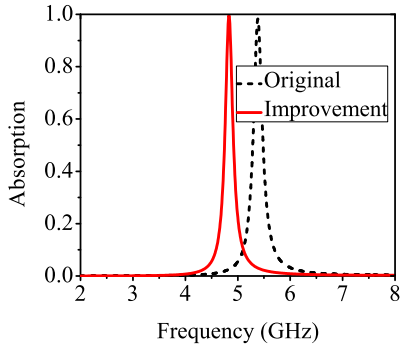

Figure 8. Calculated absorption rates of (a) original and (b) improved unit cells using the interference model.

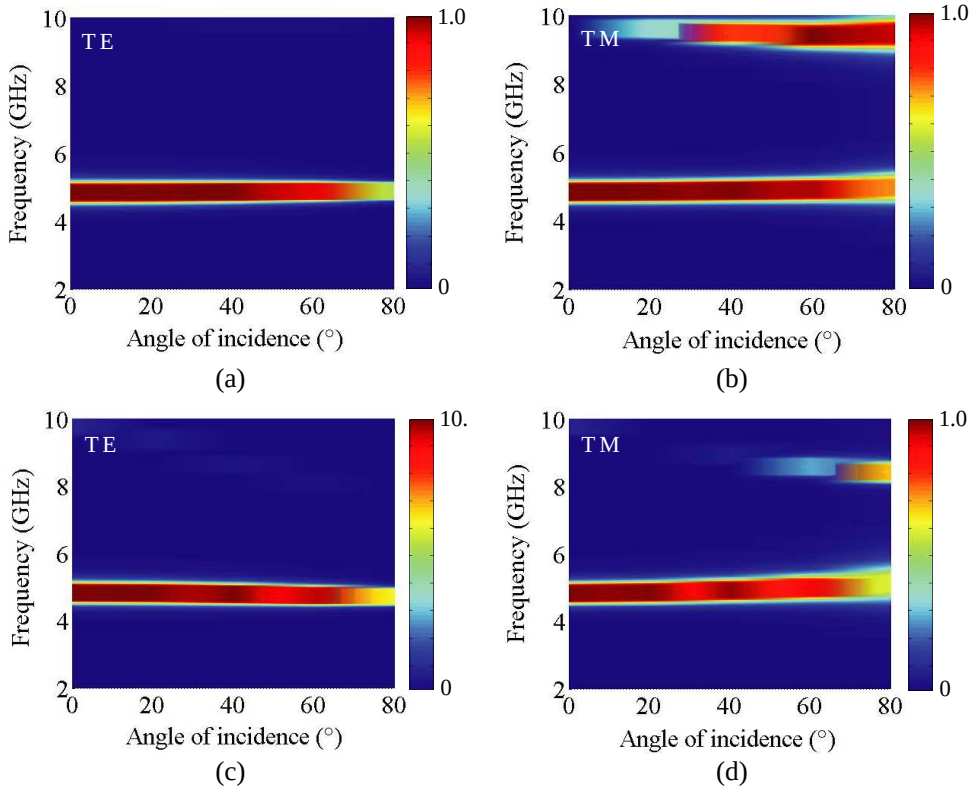

Figure 9. (a), (b) Simulated and (c), (d) calculated absorption rates of the single-band MA at different angles of incidence for TE and TM waves.

absorption peak at the frequency of about 9.40 GHz is obtained at wide incidence angles from 30° to 80°. A reduced 0.4 GHz of the resonance frequency is mainly due to the lack of the interactions between the larger-sized RSR structure and the others. Simulated results indicate that the single-band MA could work at wide angles of incidence for both TE and TM waves. Figures 9(c) and 9(d) display the calculated absorption rates of the improved unit cell using the interference model at different angles of incidence for both TE and TM waves, respectively. These calculated absorption rates for the strongly coupled MA coincide well with the simulated results at wide angles of incidence for both TE and TM waves.

4. CONCLUSION

In conclusion, we investigate the absorption rates of the triple-band MA numerically and experimentally in the microwave region. This MA is composed of a periodic array of three rotated square rings (RSRs) and a continuous metal film separated by only 1 mm dielectric substrate. The fabricated MA exhibits three absorption peaks at 4.88 GHz, 7.88 GHz, and 11.32 GHz with the corresponding absorption rates of 98.8%, 96.5%, and 95.9%, which is in excellent agreement with the simulated results. The triple-band MA is polarization-insensitive at the normal incidence. This absorber could operate well at different angles of incidence for both TE and TM waves. Finally, the multi-reflection interference theory is used to interpretate the absorption mechanism. The calculated absorption rates of the improved unit cell agree well with the simulated and experimental results. More importantly, we have successfully demonstrated that the interference theory is also effective for the strongly coupled MA at wide angles of incidence for both TE and TM waves. This proposed multi-band MA has many potential applications such as the spectroscopic detection and phase imaging of hazardous materials and prohibited drugs which require distinct absorption features at multiple frequencies.

ACKNOWLEDGMENT

This work was supported by the National Natural Science Foundation of China (Grant Nos. 10775055 and 11105002) and the Open-end Fund of State Key Laboratory of Structural Analysis for Industrial Equipment, China (Grant No. GZ1215). The authors are grateful to Dr. Houtong Chen from Los Alamos National Laboratory (USA) for helpful discussions and Prof. Rongzhou Gong from Huazhong University of Science and Technology (China) for his support in experimental measurements.

REFERENCES

1. Bilotti, F., L. Nucci, and L. Vegni, "An SRR based microwave absorber," *Microw. Opt. Techn. Let.*, Vol. 48, No. 11, 2171–2175, 2006.
2. Landy, N. I., S. Sajuyigbe, J. J. Mock, D. R. Smith, and W. J. Padilla, "Perfect metamaterial absorber," *Phys. Rev. Lett.*, Vol. 100, No. 20, 207402, 2008.
3. Zhu, B., Z. Wang, C. Huang, Y. Feng, J. Zhao, and T. Jiang, "Polarization insensitive metamaterial absorber with wide incident angle," *Progress In Electromagnetics Research*, Vol. 101, 231–239, 2010.
4. Lu, L., S. B. Qu, H. Ma, F. Yu, S. Xia, Z. Xu, and P. Bai, "A polarization-independent wide-angle dual direction absorption metamaterial absorber," *Progress In Electromagnetics Research M*, Vol. 27, 191–201, 2012.
5. Huang, Y. J., H. L. Yang, X. W. Hou, Y. Tian, and D. Y. Hou, "Perfect metamaterial absorber with dual bands," *Progress In Electromagnetics Research*, Vol. 108, 37–49, 2010.
6. He, X. J., Y. Wang, J. M. Wang, T. L. Gui, and Q. Wu, "Dual-band terahertz metamaterial absorber with polarization insensitivity and wide angle," *Progress In Electromagnetics Research*, Vol. 115, 381–397, 2011.
7. Zhu, W. R. and X. P. Zhao, "Metamaterial absorber dendritic cells at infrared frequencies," *J. Opt. Soc. Am. B*, Vol. 26, 2382–2385, 2009.
8. Zhu, W. R., X. P. Zhao, B. Y. Gong, L. H. Liu, and B. Su, "Optical metamaterial absorber based on leaf-shaped cells," *Appl. Phys. A Mater.*, Vol. 102, 147–151, 2011.

9. Wang, G. D., M. H. Liu, X. W. Hu, L. H. Kong, L. L. Cheng, and Z. Q. Chen, "Multi-band microwave metamaterial absorber based on coplanar Jerusalem crosses," *Chin. Phys. B*, Vol. 23, No. 1, 017802, 2014.
10. Huang, L. and H. Chen, "Multi-band and polarization insensitive metamaterial absorber," *Progress In Electromagnetics Research*, Vol. 113, 103–110, 2011.
11. Guo, X. R., Z. Zhang, J. H. Wang, and J. J. Zhang, "The design of a triple-band wide-angle metamaterial absorber based on regular pentagon close-ring," *Journal of Electromagnetic Waves and Applications*, Vol. 27, No. 5, 629–637, 2013.
12. Bian, B. R., S. B. Liu, H. F. Zhang, B. X. Li, and B. Ma, "A new triple-band polarization-insensitive wide-angle microwave metamaterial absorber," *PIERS Proceedings*, 435–438, Stockholm, Sweden, Aug. 12–15, 2013.
13. Shen, X. P., T. J. Cui, J. M. Zhao, H. F. Ma, W. X. Jiang, and H. Li, "Polarization-independent wide-angle triple-band metamaterial absorber," *Opt. Express*, Vol. 19, No. 10, 9401–9407, 2011.
14. Bian, B. R., S. B. Liu, S. Y. Wang, X. K. Kong, H. F. Zhang, B. Ma, and H. Yang, "Novel triple-band polarization-insensitive wide-angle ultra-thin microwave metamaterial absorber," *J. Appl. Phys.*, Vol. 114, No. 19, 194511, 2013.
15. Wang, G. D., M. H. Liu, X. W. Hu, L. H. Kong, L. L. Cheng, and Z. Q. Chen, "Broadband and ultra-thin terahertz metamaterial absorber based on multi-circular patches," *Eur. Phys. J. B*, Vol. 86, No. 7, 304, 2013.
16. Ye, Y. Q., Y. Jin, and S. L. He, "Omnidirectional, polarization-insensitive and broadband thin absorber in the terahertz regime," *J. Opt. Soc. Am. B*, Vol. 27, 498–504, 2010.
17. Cheng, Y. Z., Y. Wang, Y. Nie, R. Z. Gong, X. Xiong, and X. Wang, "Design, fabrication and measurement of a broadband polarization-insensitive metamaterial absorber based on lumped elements," *J. Appl. Phys.*, Vol. 111, No. 4, 044902, 2012.
18. Wen, D. E., H. L. Yang, Q. W. Ye, M. H. Li, L. Y. Guo, and J. F. Zhang, "Broadband metamaterial absorber based on a multi-layer structure," *Phys. Scr.*, Vol. 88, 015402, 2013.
19. Jiang, Z. H., S. Yun, F. Toor, D. H. Werner, and T. S. Mayer, "Conformal dual-band near-perfectly absorbing mid-infrared metamaterial coating," *ACS Nano*, Vol. 5, 4641–4647, 2011.
20. Hu, C. G., L. Y. Liu, Z. Y. Zhao, X. N. Chen, and X. G. Luo, "Mixed plasmons coupling for expanding the bandwidth of near-perfect absorption at visible frequencies," *Opt. Express*, Vol. 17, No. 19, 16745–16749, 2009.
21. Chen, H. T., "Interference theory of metamaterial perfect absorbers," *Opt. Express*, Vol. 20, No. 7, 7165–7172, 2012.
22. Wanghuang, T. L., W. J. Chen, Y. J. Huang, and G. J. Wen, "Analysis of metamaterial absorber in normal and oblique incidence by using interference theory," *AIP Advances*, Vol. 3, No. 10, 102118, 2013.
23. Shen, X. P., Y. Yang, Y. Z. Zang, J. Q. Gu, W. L. Zhang, and T. J. Cui, "Triple-band terahertz metamaterial absorber: Design, experiment, and physical interpretation," *Appl. Phys. Lett.*, Vol. 101, No. 15, 154102, 2012.
24. Huang, L., D. R. Chowdhury, S. Ramani, M. T. Reiten, S. N. Luo, A. K. Azad, A. J. Taylor, and H. T. Chen, "Impact of resonator geometry and its coupling with ground plane on ultrathin metamaterial perfect absorbers," *Appl. Phys. Lett.*, Vol. 101, No. 10, 101102, 2012.
25. Padilla, W. J., M. T. Aronsson, C. Highstrete, M. Lee, A. J. Taylor, and R. D. Averitt, "Electrically resonant terahertz metamaterials: Theoretical and experimental investigations," *Phys. Rev. B*, Vol. 75, No. 4, 041102, 2007.